ARMY RESEARCH LABORATORY

Lagrangian Modeling of Evaporating Sprays at Diesel Engine Conditions: Effects of Multi-Hole Injector Nozzles With JP-8 Surrogates

by L. Bravo, M. Kurman, C. Kweon, S. Wijeyakulasuriya, and P. K. Senecal

ARL-RP-486   **June 2014**

NOTICES

Disclaimers

The findings in this report are not to be construed as an official Department of the Army position unless so designated by other authorized documents.

Citation of manufacturer's or trade names does not constitute an official endorsement or approval of the use thereof.

Destroy this report when it is no longer needed. Do not return it to the originator.

Army Research Laboratory
Aberdeen Proving Ground, MD 21005-5066

ARL-RP-486   **June 2014**

Lagrangian Modeling of Evaporating Sprays at Diesel Engine Conditions: Effects of Multi-Hole Injector Nozzles With JP-8 Surrogates

L. Bravo, M. Kurman, and C. Kweon
Vehicle Technology Directorate, ARL

S. Wijeyakulasuriya and P. K. Senecal
Convergent Science, Inc.

REPORT DOCUMENTATION PAGE

Form Approved
OMB No. 0704-0188

1. REPORT DATE *(DD-MM-YYYY)*	2. REPORT TYPE	3. DATES COVERED (From - To)
June 2014	Reprint	January–March 2014

4. TITLE AND SUBTITLE	5a. CONTRACT NUMBER
Lagrangian Modeling of Evaporating Sprays at Diesel Engine Conditions: Effects of Multi-Hole Injector Nozzles With JP-8 Surrogates	
	5b. GRANT NUMBER
	5c. PROGRAM ELEMENT NUMBER

6. AUTHOR(S)	5d. PROJECT NUMBER
L. Bravo, M. Kurman, C. Kweon, S. Wijeyakulasuriya, and P. K. Senecal	
	5e. TASK NUMBER
	5f. WORK UNIT NUMBER

7. PERFORMING ORGANIZATION NAME(S) AND ADDRESS(ES)	8. PERFORMING ORGANIZATION REPORT NUMBER
U.S. Army Research Laboratory ATTN: RDRL-VTP Aberdeen Proving Ground, MD 21005-5066	ARL-RP-486

9. SPONSORING/MONITORING AGENCY NAME(S) AND ADDRESS(ES)	10. SPONSOR/MONITOR'S ACRONYM(S)
	11. SPONSOR/MONITOR'S REPORT NUMBER(S)

12. DISTRIBUTION/AVAILABILITY STATEMENT

Approved for public release; distribution is unlimited.

13. SUPPLEMENTARY NOTES

14. ABSTRACT

Numerical modeling of the evaporation process in sprays under diesel conditions is key for the development of efficient injection strategies and to increase combustion efficiency. In this study, three-dimensional numerical simulations of single and two-hole injector nozzles under diesel conditions are conducted to study the spray behavior and the effect of multi-hole nozzles on heavy fueled spray parameters and mixing. The configuration corresponds to a high-pressure JP-8 spray injected into a high temperature pressure vessel (HTPV) flow-through combustion chamber simulating realistic conditions found in diesel engines. A Lagrangian particle tracking method coupled with a classical blob injection wave-based model is adopted through the use of CONVERGE solver to treat the spray process. An Adaptive Mesh Refinement (AMR) and fixed embedding technique is employed to capture the gas-liquid interface with high fidelity while keeping the cell-count reasonable. Two JP-8 liquid fuel surrogates, Surrogate-C (of 60% n-dodecane, 20% methylcyclohexane, 20% o-xylene), and the Modified Aachen surrogate (80% n-dodecane and 20% trimethylbenze) were interrogated resulting in good agreement with high fidelity spray measurements. Spray simulation results are compared to our in-house experimental data for JP-8 with single axial hole and two-hole adjacent (60°) nozzle configurations. Standardized Engine Combustion Network (ECN) Spray A ambient conditions, consisting of 900 K and 60 bar, are selected with a rail pressure of 1000 bar with nominal nozzle diameter $d_j = 147\ \mu m$. Utilizing $k - \epsilon$ Reynolds-Average Navier Stokes, and dynamic structure Large Eddy Simulation methodologies both configurations result in a 20 mm mean liquid length for both single and two hole cases. This is in good agreement with experiments with the single, while for the double hole this is an over-prediction of 3-5 mm. The reported differences are partially attributed to the internal nozzle flow dynamics, reported nozzle eccentricities, the influence of these effects are discussed.

15. SUBJECT TERMS

multiphase flows, LES, RANS, VOF, JP-8, surrogate fuels, turbulence

16. SECURITY CLASSIFICATION OF:			17. LIMITATION OF ABSTRACT	18. NUMBER OF PAGES	19a. NAME OF RESPONSIBLE PERSON
					L. Bravo
a. REPORT	b. ABSTRACT	c. THIS PAGE	UU	22	19b. TELEPHONE NUMBER *(Include area code)*
Unclassified	Unclassified	Unclassified			410-278-9525

Standard Form 298 (Rev. 8/98)
Prescribed by ANSI Std. Z39.18

Lagrangian Modeling of Evaporating Sprays at Diesel Engine Conditions: Effects of Multi-Hole Injector Nozzles with JP-8 Surrogates

L. Bravo[*], M. Kurman, C. Kweon
U.S. Army Research Laboratory
Aberdeen Proving Ground, MD USA

S. Wijeyakulasuriya , P.K. Senecal
Convergent Science, Inc
Middleton, WI, USA

Abstract

Numerical modeling of the evaporation process in sprays under diesel conditions is key for the development of efficient injection strategies and to increase combustion efficiency. In this study, three-dimensional numerical simulations of single and two-hole injector nozzles under diesel conditions are conducted to study the spray behavior and the effect of multi-hole nozzles on heavy fueled spray parameters and mixing. The configuration corresponds to a high-pressure JP-8 spray injected into a high temperature pressure vessel (HTPV) flow-through combustion chamber simulating realistic conditions found in diesel engines. A Lagrangian particle tracking method coupled with a classical blob injection wave-based model is adopted through the use of CONVERGE solver to treat the spray process. An Adaptive Mesh Refinement (AMR) and fixed embedding technique is employed to capture the gas-liquid interface with high fidelity while keeping the cell-count reasonable. Two JP-8 liquid fuel surrogates, Surrogate-C (of 60% n-dodecane, 20% methylcyclohexane, 20% o-xylene), and the Modified Aachen surrogate (80% n-dodecane and 20% trimethylbenze) were interrogated resulting in good agreement with high fidelity spray measurements. Spray simulation results are compared to our in-house experimental data for JP-8 with single axial hole and two-hole adjacent (60°) nozzle configurations. Standardized Engine Combustion Network (ECN) Spray A ambient conditions, consisting of 900 K and 60 bar, are selected with a rail pressure of 1000 bar with nominal nozzle diameter $d_j = 147\ \mu m$. Utilizing $k - \epsilon$ Reynolds-Average Navier Stokes, and dynamic structure Large Eddy Simulation methodologies both configurations result in a 20 mm mean liquid length for both single and two hole cases. This is in good agreement with experiments with the single, while for the double hole this is an over-prediction of 3-5 mm. The reported differences are partially attributed to the internal nozzle flow dynamics, reported nozzle eccentricities, the influence of these effects are discussed.

_____

[*]Corresponding author: luis.g.bravo2.ctr@mail.mil

Introduction

In many combustion systems, fuel atomization and the spray breakup processes play an important role in determining combustion characteristics and emissions formation. Due to the ever rising need for greater fuel efficiency and lower emissions, the development of a fundamental understanding of its process is essential and remains a challenging task. In U.S. military unmanned aerial system (UAS) and unmanned ground system (UGS) applications, the characterization of engines operating with JP-8 aviation fuel is vital to understand engine performance, combustion phasing, and emissions when JP-8 is fully substituted for diesel fuel [1]. This emerges from the Department of Defense (DOD)'s "Single Fuel Forward" policy requiring military vehicles, and equipment to be capable of using a single battlefield fuel [1]. Hence, characterization of JP-8 spray and combustion will remain of critical priority in enabling the Army mission while facilitating fuel logistics operations.

In recent years, the engine modeling community has relied on the Engine Combustion Network (ECN) as the premier research consortium to validate physical/chemical models and demonstrate several numerical features of CFD solvers. ECN group includes multi-institutional facilities leveraging expertise and characterizing diesel and gasoline sprays through use of optically accessible, constant-volume combustion vessels under simulated, quiescent diesel engine conditions [2-3]. Much of the modeling work is aimed at demonstrating features important for multiphase 3D-CFD solvers such as: the ability to accurately describe Lagrangian particles in Eularian gas phase models, assess the performance of leading turbulence models, model combustion through adequate surrogate selection; and numerically to obtain grid convergent simulations with low-to-high fidelity models of global spray and combustion properties [4], [5].

Using a RANS technique, Som et al [5] conducted several validation studies and presented an assessment of leading Lagrangian/Eularian atomization models in diesel non-reacting sprays. Some discrepancies in the atomization models were reported for non-evaporating spray conditions in terms of the dispersion behavior while this effect was not as pronounced in evaporating sprays where good agreements were obtained. It also was recognized that atomization is strongly influenced by upstream conditions arising from internal flow cavitation, turbulence, and nozzle geometry. The fidelity of the rate-of-injection profiles was also shown to be critical to correctly predict the spray behavior for validation purposes. More recently and extending this work, Senecal et al [6] has reported in detail the modeling guidelines to simulate non-evaporating, evaporating, and reacting diesel sprays utilizing the CONVERGE solver in single-hole configurations. In this study, nominal ECN Spray A conditions were used to demonstrate key modeling features to enable grid converged calculations, such as the importance of adaptive-mesh-refinement (AMR), fixed grid embedding, and the proper use of Lagrangian parcel distribution for accurate hydrodynamic representation of the multiphase flow [6].

Further studies demonstrated the effect of several high-resolution LES turbulence techniques on resolving the flow field, cycle to cycle variations in the context of grid convergence, and its effect on spray modeling constants [7-8]. Good agreement was found for global quantities such as liquid and vapor penetration lengths with experimental data for single-shot LES realization. However, deeper comparison to local quantities such as velocity and mixture fraction was shown to require the average of many additional LES realizations. Moreover, the spray breakup constants are demonstrated to also depend on the amount of resolution utilized in resolving the flow fields, hence the transition from RANS to LES models was reported to require consideration to recalibrate. Similarly, Habchi et al [9] studied the effects of LES ensemble averaging using single-hole injectors in high-pressure, high-temperature vessel and found good agreements with experimental data using 10-30 LES realizations using the AVBP solver. Hence, it is generally agreed that using LES is similar to a single-shot experimental injection requiring ensemble averaging, while with RANS a single shot realization will be enough to capture important spray quantities albeit with lower accuracy.

The aim in this study is to extend the present modeling scope to multi-hole nozzles at the standardized ECN conditions. Its merit also includes introducing the use of surrogate fuel mixtures to model evaporating JP-8 evaporating sprays at diesel conditions. Grid converged numerical calculations are sought in order to provide grid criteria in single and multi-hole nozzle configurations. The models were added to the present CONVERGE liquid fuel database and validated extensively leveraging the DOD's Spray Combustion Research Lab (SCRL) at ARL-VTD. The measurements and the experimental facility are presented in more details in the work of Kurman et al [10].

Numerical Method

The CONVERGE 3D-CFD solver, developed by Convergent Science Inc (CSI), has been adopted in this study to perform detailed spray simulations at realistic engine operating conditions. CONVERGE is a compressible Navier Stokes solver which is based on a first order predictor-corrector (PISO) time integration scheme, and a choice of second or higher order finite volume schemes for spatial discretization. It features a non-staggered, collocated, computation grid framework

utilizing a Rhie-Chow interpolation technique to avoid spurious oscillations. An efficient geometric multi-grid treatment is used to solve the pressure equation, and parallel computing is based on implementations of either OpenMP or Message Passing Interface (MPI) protocols. It provides the option of increasing resolution locally through static fixed-grid embedding, and dynamically through AMR activated through user specified criteria. Additionally, it uses state-of-the-art Eularian-Lagrangian spray models, and a parallel detailed chemistry solver for combustion that can be fully coupled with CHEMKIN databases. The solver also provides a choice between a number of modeling options for the treatment of turbulence, including direct numerical simulation (DNS), large eddy simulation (LES) and Reynolds-averaged Navier-Stokes (RANS).

Dynamic Structure LES Model (DSLES)

In this study, the gas phase is described using the Favre Averaged Navier Stokes Equations while adopting the dynamic structure LES model (DSLES) [11-12]. The compressible system of transport equations for mass, momentum and energy are presented here in a LES framework,

$$\frac{\partial \bar{\rho}}{\partial t} + \frac{\partial \bar{\rho} \tilde{u}_j}{\partial x_j} = 0 \tag{1}$$

$$\frac{\partial \bar{\rho} \tilde{u}_i}{\partial t} + \frac{\partial \bar{\rho} \tilde{u}_i \tilde{u}_j}{\partial x_j} = -\frac{\partial \bar{P}}{\partial x_i} + \frac{\partial \overline{\sigma_{ij}}}{\partial x_j} - \frac{\partial \tau_{ij}}{\partial x_j} \tag{2}$$

where the subgrid stress tensor is given by

$$\tau_{ij} = \bar{\rho} \left(\widetilde{u_i u_j} - \tilde{u}_i \tilde{u}_j \right) \tag{3}$$

In the DSLES methodology, the subgrid stress tensor is modeled through a non-viscosity based one-equation LES model. The transport equation for the subgrid kinetic energy is written as,

$$\frac{\partial \bar{\rho} k}{\partial t} + \frac{\partial \bar{\rho} \widetilde{u_j} k}{\partial x_j} = \frac{\partial}{\partial x_j} \left(\frac{\mu}{\text{Pr}_{\text{sgs}}} \frac{\partial k}{\partial x_j} \right) + \tau_{ij} \overline{S_{ij}} - \bar{\rho} \epsilon \tag{4}$$

where the subgrid kinetic energy is given by,

$$k = \frac{1}{2} \left(\widetilde{u_i u_j} - \tilde{u}_i \tilde{u}_j \right) \tag{5}$$

and the subgrid dissipation rate is given by,

$$\epsilon = \frac{C_\epsilon k^{1.5}}{\Delta} \tag{6}$$

Model constants in this formulation is $C_\epsilon = 1$, Δ represents the local grid length scale, $\overline{S_{ij}}$ is the filtered strain rate and Pr_{sgs} is set 1.39. The subgrid stress tensor is now modeled as,

$$\tau_{ij} = 2k\bar{\rho} \frac{L_{ij}}{L_{kk}} \tag{7}$$

where the Leonards stress tensor is classically defined as, $L_{ij} = \left(\widehat{\tilde{u}_i \tilde{u}_j} - \widehat{\tilde{u}_i} \widehat{\tilde{u}_j} \right)$ including the test filter and grid filter level in its definition.

DSLES methodology requires the scalar and energy transport equations be written using the eddy viscosity concept,

$$\frac{\partial \bar{\rho} \overline{Y_m}}{\partial t} + \frac{\partial \bar{\rho} \bar{u}_j \overline{Y_m}}{\partial x_j} = \frac{\partial}{\partial x_j} \left(\bar{\rho}(D + D_t) \frac{\partial \overline{Y_m}}{\partial x_j} \right) \tag{8}$$

where $D_t = C_k k^{0.5}/Sc$ defines the turbulent diffusion parameter with $C_k = 0.5$ and Schmidt number $Sc = 0.78$.

Time Advancement

Equations (1) and (2) are solved numerically using a classical predictor-corrector scheme in which the velocity field is first integrated using the Navier Stokes equation (2) and then corrected to enforce mass conservation (1) using a modified pressure. This is achieved using the modified Pressure Implicit with Splitting of Operator (PISO) algorithm first introduced by Issa [13].

An illustration of the PISO predictor-corrector sequence is presented below (note that H^* represents convection, diffusion, S accounts for implicit/explicit sources, and * denotes the intermediate steps) for a one-time correction procedure,

Predictor step:

$$\frac{\rho^n u_i^*}{\partial t} - \frac{\rho^n u_i^n}{\partial t} = -\frac{\partial P^n}{\partial x_i} + H_i^* \tag{9}$$

Corrector step:

$$\frac{\rho^* u_i^{**}}{\partial t} - \frac{\rho^n u_i^n}{\partial t} = -\frac{\partial P^*}{\partial x_i} + H_i^* \tag{10}$$

$$\frac{\partial^2}{\partial x_i \partial x_i} (P^* - P^n) - \frac{(P^* - P^n)\phi}{dt^2} = \left(\frac{\partial \rho^n u_i^*}{\partial x_i} - S \right) \frac{1}{dt}$$

Update step:

$$\frac{\rho^* u_i^{**}}{\partial t} - \frac{\rho^n u_i^*}{\partial t} = -\frac{\partial}{\partial x_i} (P^* - P^n) \tag{11}$$

3

where dt is the numerical integration time step. Once the pressure is solved, the velocity is re-calculated according to the updated momentum equation.

Physical Spray Models

Spray modeling is treated using the "blob" injection method of Reitz and Diwakar [14]. Blobs of a characteristic size are injected following a statistical distribution into the computational domain. Primary and secondary breakups are subsequently simulated based on the Kelvin-Helmholtz (KH) and Rayleigh-Taylor (RT) instability methods. Note that the breakup length is not determined a-priori (breakup length concept) and is calculated as a part of the solution.

In the KH wave model, atomization is treated using stability analysis for liquid jets. The breakup of the injected blobs and resulting drops of radius r_o is calculated by assuming that the drop radius is proportional to the wavelength of the fastest growing unstable surface wave Λ_{KH}.

It is written as, $r = B_0\Lambda_{KH}$, where B_0 is a model constant. Droplet size, and its rate of change is calculated as,

$$\frac{dr_0}{dt} = -\frac{(r_0 - r)}{\tau_{KH}} \qquad (12)$$

where the breakup time constant, τ_{KH} , is calculated as,

$$\tau_{KH} = \frac{3.726 B_1 r_0}{\Lambda_{KH}\Omega_{KH}} \qquad (13)$$

and the maximum growth rates Ω_{KH} and corresponding wavelengths Λ_{KH} have been simplified and defined as follows,

$$\Omega_{KH}\left(\frac{\rho_l a^3}{\sigma}\right) = \frac{0.34 + 0.38 We_g^{1.5}}{(1 + Z)(1 + 1.4T^{0.6})} \qquad (14)$$

$$\frac{\Lambda_{KH}}{a} = 9.02\frac{(1 + 0.45Z^{0.5})(1 + 0.4T^{0.7})}{\left(1 + 0.87 We_g^{1.67}\right)^{0.6}} \qquad (15)$$

where,

$$Z = We_l^{0.5}/Re_l \, , T = We_g^{0.5}, We_l = \rho_l U^2 a/\sigma \, ,$$
$$We_g = \rho_g U^2 a/\sigma, \text{ and } Re_l = Ua/\nu_l$$

The present Rayleigh-Taylor mechanism formulation includes viscosity variations in the growth rate equation,

$$\omega_{RT} = -k_{RT}^2 \left(\frac{\mu_l + \mu_g}{\rho_l + \rho_g}\right) + \dots \qquad (16)$$

$$\dots \sqrt{k_{RT}\left(\frac{\rho_l - \rho_g}{\rho_l + \rho_g}\right) a - \frac{k_{RT}^3 \sigma}{\rho_l + \rho_g} + k_{RT}^4 \left(\frac{\mu_l + \mu_g}{\rho_l + \rho_g}\right)^2}$$

where k_{RT} is the wavenumber, μ_l is the liquid viscosity, μ_g is the gas viscosity, ρ_l is the liquid density, ρ_g the gas density, a is the deceleration of the drop, and σ is the liquid surface tension. The wave number corresponding to the maximum growth rate $K_{RT} = 2\pi/\Lambda_{RT}$ is calculated through a bisection method with equation (16). The value is updated to calculate the maximum growth rate Ω_{RT}. The predicted RT model drop size is then expressed as,

$$r_{RT} = C_{RT}\Lambda_{KH} \qquad (17)$$

where C_{RT} is the model constant, and Λ_{KH} is the predicted RT wavelength. In summary the spray model constants used in this study are defined as: $B_0 = 0.6$, $B_1 = 10$, $C_{RT} = 0.1$, and $C_\tau = 1$.

Lastly, other spray processes that were modeled include droplet distortion and drag, droplet interactions in terms of collision and coalescence, turbulent dispersion, and evaporation. The two phases are coupled through the exchange of mass, momentum, and energy, represented in the appropriate source terms in the gas-phase equations. These models are reviewed and described in detail in a recent report by Bravo et al and the reader is referred to that article [15].

Experimental Data and Computational Setup

Model validation is carried out with our in-house database at ARL-VTD, Spray Combustion Research Laboratory (SCRL). This is a state-of-the-art facility housing a HTPV providing the high temperature and high pressure thermodynamic conditions obtained in a diesel engine. Unlike CVP (Constant Volume Preburn) vessels this rig does not require a pre-burn phase to obtain this condition and rather it is comprised of four subsystems including: gas compressor, gas heater, test vessel, and control system to achieve nearly quiescent and steady thermodynamic conditions. An onsite nitrogen generator (Model N-350 PSA) and a high-pressure compressor (Sauer Model WP4351) continuously deliver high-pressure nitrogen to the HTPV. A 2-stage cartridge electrical heater and a ceramic heater are used to increase the gas temperature with the use of a control system (closed loop PID) to adjust for both the chamber pressure and the power of the heater to obtain homogenous temperature conditions. To characterize the liquid and vapor global

measurements an advanced optical set up with an LED array is used for Mie scattering technique and single LED lighting is used for schlieren technique. Bosch common-rail fuel injectors with $147\ \mu m$ nominal diameter were used in experiments. X-ray CT scan images of the injectors are shown in Figure1.

Parameter	Quantity	
Injector Types	BOSCH CRIN3	
Number of Holes	1	2
Nominal Orifice Diameter (μm)	147	147
Fill Gas	N_2 99%	
Chamber Density (kg/m^3)	22.8	
Chamber pressure (bar)	60	
Fuel	JP-8	
Fuel Temperature (K)	373	
Fuel injection Quantity (mg)	7.05	11.52
Injection Pressure (bar)	1000	
Injection Duration (ms)	1.1	
Pulse Duration (ms)	0.7	

Table 1. Test matrix combustion vessel and fuel injector with experimental conditions for CFD model validation.
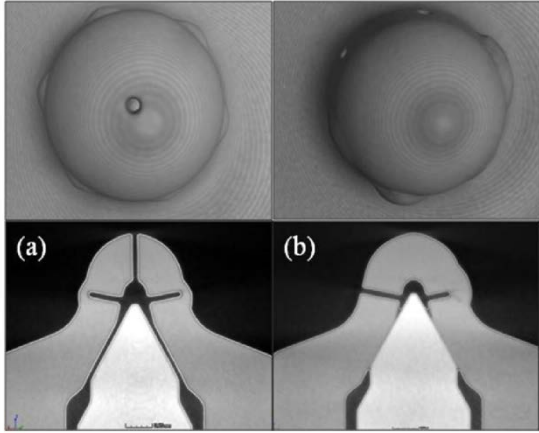

Figure 1. Rendered X-ray CT scans (top row) with corresponding image slices (bottom row) for single (a) and two-hole (b) injectors.

It is noted that the single-hole nozzle orifice presented in Figure 1a has been manufactured using wire-EDM technique while welding shut the side orifices. The top row is a rendered image from the CT scan showing that the orifice is not aligned with axial position. Two-hole nozzle orifices also have welding on the side orifices to allow control of the fuel injection orifices. The nominal distance between orifices in this case is approximately 1 mm with 60 degree internal angle as shown in the Figure 1b. The images in Figure 1

are insightful in presenting manufacturing eccentricities that are useful for full understanding of the spray behavior.

To characterize the rate of injection (ROI) and the injected fuel mass, each fuel injector was tested in an IAV fuel injection analyzer. For the injector characterization presented in this work, a 100 shot average was acquired for the injected fuel mass, ROI, and current profile. The ROI profiles used in the CFD work and their comparison to experiments are presented in Figure 2. Other operating conditions used in this study are provided in Table 1.
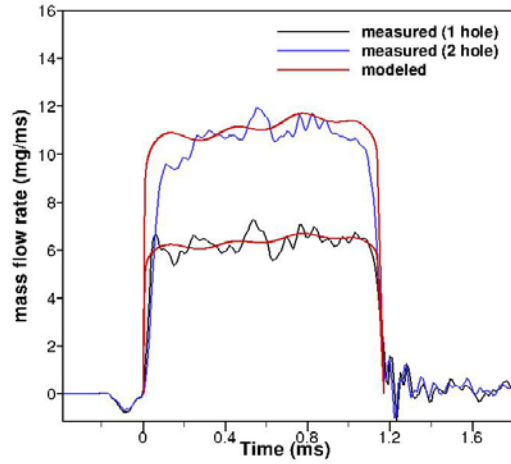

Figure 2. Experimental Rate of Injection Profiles compared with the profiles used in CFD work.

In this study we use numerical simulations to model transient non-reacting JP-8 sprays under diesel engine conditions. The CONVERGE multiphase solver is used invoking a classical Lagrangian/Eularian formulation to treat the gas-phase and liquid phase with wave-based spray models. The study includes single-hole and two-hole nozzle configurations at the nominal Spray A ambient conditions.

There are several important procedures to be mindful when running spray simulations. First, an AMR procedure must be adopted to control the refinement levels in the vicinity of the spray. Figure 3 shows the effects of AMR refinements in the near the spray calculated with a velocity criteria using a base grid of 2 mm. In this study, AMR is activated for the velocity field and its use is critical in keeping the cell counts at realistic operating levels. Note also that fixed grid embedding (in spray liquid core region) is used to define the reference minimum cell sizes, dx, and the embedding scale. The parameters are related through the base grid cell size, dx_{base}, as follows: $dx = dx_{base}/(dx_{base}^{escale\_level})$. The coarsest base grid cell size of 2 mm, and an embed scale of 3 corresponds to dx=0.25 mm. When conducting grid refinements, the

number of injected particles must be increased at each refinement level. Using a fixed number of injected particles will lead to an artificial increase of the liquid penetration length as was reported in a previous study by Senecal et al [6]. This is due to the decrease of relative gas to liquid mass that occurs in each cell as the mesh is refined. Overlooking this can artificially cause the gas velocity to approach the particle velocity at every cell leading to an artificial decrease in particle drag.
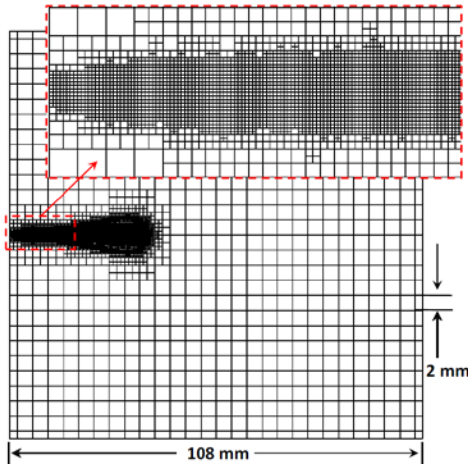

Figure 3. Computational mesh showing the effects of AMR near the spray region, and a coarse base mesh outside of it.

Table 2 documents the number of resolution levels, denoted as embedding scale, and the critical number of injected particles used in grid-sensitivity analysis. Embed scales 3-5 were used in this study.

Embed Scale	Cell Size dx(mm)	d_n/dx_i	Injected Parcels
2	0.5	0.294	12,500
3	0.25	0.588	50,000
4	0.125	1.176	200,000
5	0.0625	2.352	800,000

Table 2. AMR embed scale (column 1), cell sizes (column 2), number of cells inside of the nozzle diameter (column 3), and number of injected parcels (column 4) used for evaporating sprays.

The guidelines above were utilized in conducting grid convergence studies to demonstrate the numerical accuracy of the model. Numerical convergence can be achieved at cell sizes 0.125 mm (1 hole) and 0.0625 mm (2 hole) configurations. Physical validation is conducted by comparing grid-converged results to the measurements. In this study both liquid and vapor penetration data was available for this task as well as animations showing plume structure.

Overview and Selection of JP-8 Surrogate Fuel

There exist several categories of aviation fuels in operation ranging from commercial aviation fuels, including Jet A and Jet A-1, to military jet fuels using a different classification system JP numbers spanning from JP-1 to JP-8 varying with application [16]. A general summary of fuel property data is given by Edwards et al. in his review of relevant military fuels [17]. Fuel JP 4 is reported as a gasoline/kerosene blend used by the U.S. Air Force (USAF) until the 1980's when it was replaced by JP-8; a kerosene based fuel. JP-8's specifications are similar to Jet A (Jet A-1), which is a commercial aviation kerosene fuel, with the difference due to the addition of three additives; the additives are: a lubricity improver/corrosion inhibitor, antistatic additive, and a fuel system icing inhibitor. Fuel JP-5 is a high flash-point kerosene used for aircraft flying from U.S. Navy ships, while fuel JP-7 is an exclusive kerosene fuel developed for supersonic applications related to the military SR-71 "Blackbird" aircraft. The following table lists average property data for the aforementioned military fuels [17].

Property	JP-4	JP-7	JP-8
Approx formula	$C_{8.5}H_{17}$	$C_{12}H_{25}$	$C_{11}H_{21}$
H/C ratio	1.99	2.02	1.91
Boil Range, F	140-460	370-480	330-510
Freeze Point, F	-80	-47	-60 JP8/JetA1 -50 Jet A
Flash point, F	-10	140	127
Net heating val (BTU/lb)	18,700	18,530	18,580
Specific gravity 60 F	0.76	0.79	0.81
Critical T, F	450	305	340
Critical P, psia	450	305	340
Average comp.			
aromatics, vol%	10	19	18
naphthenes	29	32	20
paraffins	59	65	60
olefins	2	--	2
sulfur, ppm	370	60	490

Table 3. Bulk fuel properties of typical aviation military fuels (Edwards et al [16]).

An inspection of Table 2 reveals that the major hydro-carbon constituents found in JP-8 are: paraffins, 60 vol%, followed by naphthenes (cycloparaffins), 20 vol%. It is reported that paraffins are composed of

primarily of straight-chained or branched molecules, with mono-cycloparaffins also being significant. A major paraffin component is usually n-decane or n-dodecane, characterized with high H/C ratios and high energy release rates per unit weight. Naphthenes have lower H/C ratios and exhibit lower gravimetric heating values; however, they feature higher volumetric energy densities and lower freezing points providing operational advantages. Aromatic content in JP-8 fuel is of 18 vol% and constitutes the third largest class of compounds. Aromatic hydrocarbons can be monocyclic (MAH) and polycyclic (PAH), where polycyclic-aromatic hydrocarbons are well-known soot precursors and is an undesirable result of incomplete combustion directly affecting engine performance. Government regulations for aviation fuels limit the aromatic content in JP-8 to be around 18% - 25%. Lastly, trace species such as sulfur and metals is important in fuels for thermal stability and emissions. The average sulfur content among JP-8 fuels is tabulated as 490 ppm (0.049 mass%), less than the 0.3 mass% government mandated maximum.

Surrogate-C		$\mathcal{M}_i$	χ_i	y_i
n-dodecane	$C_{12}H_{26}$	170	0.6	0.714
Methylcy-clohexane	C_7H_{14}	98	0.2	0.137
o-xylene	C_8H_{10}	106	0.2	0.148
H/C ratio	1.97		$\mathcal{M}_{mix}$	142.8
Surrogate-Mod Aachen		$\mathcal{M}_i$	χ_i	y_i
n-dodecane	$C_{12}H_{26}$	170	0.8	0.85
trimethyl-benzene	C_9H_{12}	120	0.2	0.15
H/C ratio	1.99		$\mathcal{M}_{mix}$	160

Table 4. Table 4. JP-8 surrogate composition. Chemical formula (column 2), molecular weight (column 3), mole fraction (column 4), mass fraction (column 5). Note the last rows provide each surrogate H/C ratio and molecular weight.

In this study, the use of surrogate fuels is adopted in an effort to model JP-8 liquid physical properties. A literature review reveals that there is a need for a complete characterization of JP-8 liquid phase

properties (i.e., vapor pressure) that spans an extensive temperature range for use in CFD models. The models used in this study were selected based on literature review on gas-phase JP-8 surrogates and their availability [16]. They are a two-component Modified Aachen surrogate with constituents of n-dodecane and trimethylbenze, and a three-component Surrogate-C with constituents of n-dodecane, o-xylene, and methylcyclohexane. The exact mole and mass-fraction compositions, mixture molecular weight and hydrogen to carbon ratios (H/C) are presented in Table 4.

Results and Discussion

In this section we present modeling results of JP-8 evaporating spray simulations with single-hole and two-hole nozzle configurations at the Spray A ambient conditions. Using a RANS approach we compare the spray global parameters, liquid and vapor penetration profiles, and study the effect of resolution and surrogate fuels on spray structure. With the LES approach we investigate further the turbulent flow field mixing behavior surrounding the atomizing jet through visualization of velocity profiles, vorticity, and mixture fraction.

For reference, the calculations of liquid and vapor penetrations for simulations are defined as follows:

Parameter	Definition
Liquid Penetration	Axial distance encompassing 97% of the injected liquid fuel mass.
Vapor Penetration	Maximum axial distance from the injector orifice where the fuel mass fraction $Y_f = 0.1\%$.

Table 5. Definitions of current evaporating spray global parameters.

Surrogate Grid Convergence (Single-Hole Nozzle)

Of interest here is to develop a model in which the global diagnostics presented above asymptotically converge as the mesh is refined. Grid convergence in this study has been achieved by utilizing the solver's ability to refine the grid dynamically by using AMR, and locally by use of fixed grid embedding modules. A correct representation of the particle hydrodynamics is also important in predicting the spray behavior. This is achieved by increasing the number of injected particles with resolution level. The convergence grid parameters selected here correspond to grid cell sizes of $dx = 0.25, 0.125, 0.0625\ mm$. In this case, the relative nozzle-to-cell ratio increases approximately by two with each level reaching a peak value of $d_n/dx = 2.352$ for $dx = 0.0625\ mm$.

The first set of grid sensitivity results are conducted with Surrogate-C showing good comparison

to measurements for liquid and vapor penetration profiles as seen in Figure 4a-b. In Figure 4a (top), for a cell size $dx = 0.25\ mm$, there is a sharp peak in the transient region of the liquid penetration profiles. This unphysical spike in penetration is a clear indicator of unresolved grid effects. Improvements are gradually obtained for cells $dx = 0.125,\ 0.0625\ mm$ where the finer grid removes the peak and hence is able to capture the transient spray behavior more accurately. Surrogate-C vapor penetration behavior also shows asymptotically convergence behavior as resolution is increased, see Figure 4b (bottom). In this case, grid effects become evident after a time of 0.2ms. Some of the reported discrepancies with the present vapor phase length are attributed to the uncertainties in the numerical length calculation.
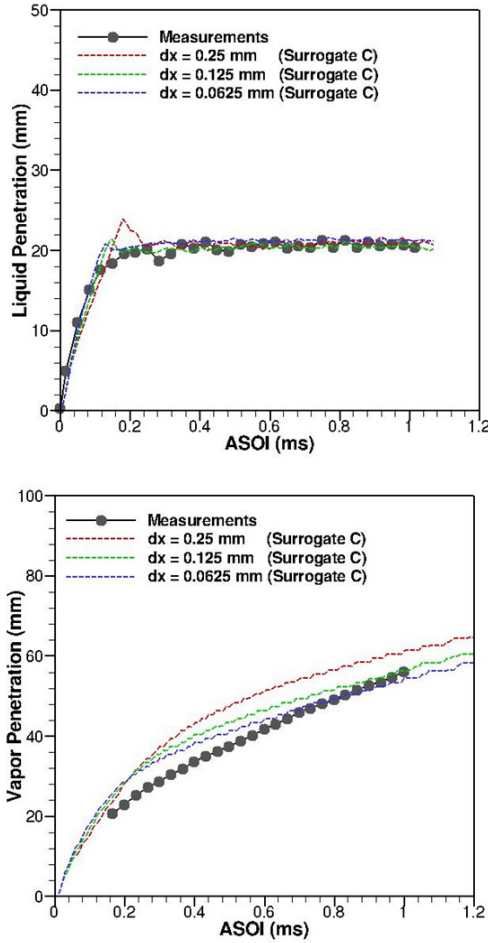
Figure 4. Surrogate-C, single hole nozzle, grid convergence behavior with liquid (a) and vapor (b) penetration profiles.

A further study utilizing the Modified Aachen surrogate shows similar results as with Surrogate-C in terms of the liquid and vapor profiles, Figures 5a-b. The similarities in physical behavior for each surrogate can be attributed to its small variance (less than 2%) while both values are near the JP-8 reported value $H/C = 1.99$. It is also important to note that the temporal breakup constant, B_1, was recalibrated to represent the present spray behavior with JP-8 (repeated here for clarity) $\tau_{KH} = 3.726 B_1 r_0 / \Lambda_{KH} \Omega_{KH}$ This was achieved by carrying out a parametric study with B_1 and selecting the best approximation with experiments. In this process the breakup constant was modified for JP-8 surrogates from $B_1 = 7$ (diesel fuels) to $B_1 = 10$.
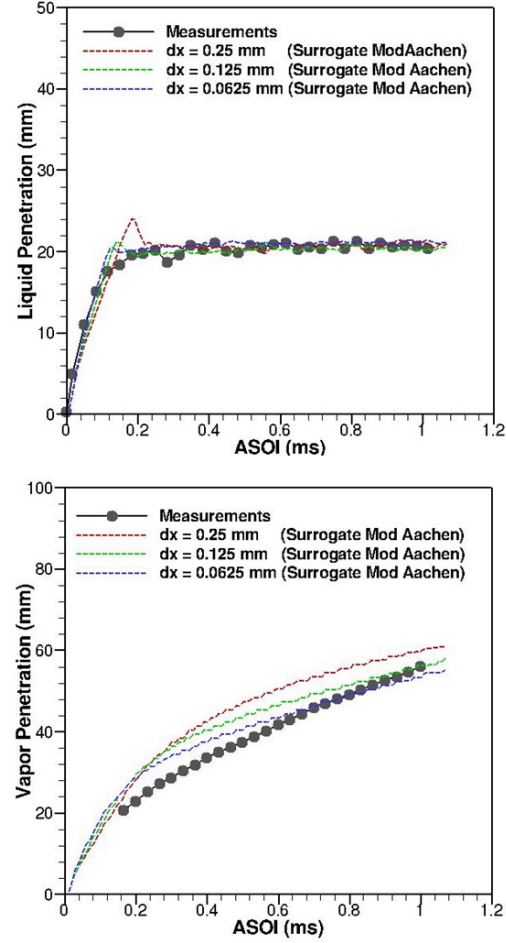

Figure 5. Surrogate-Modified Aachen, single hole nozzle, grid convergence behavior with liquid (a) and vapor (b) penetration profiles.

Figure 6 presents the computed spray structure at times 50, 100, and 200 μs after start of injection at a resolution level $dx = 0.0625$. The vertical line marks the computed (RANS) liquid lengths. Note that the RANS turbulence model adopted in this study captures very well the transient and steady penetration behavior; however, higher fidelity is needed to capture the mixing spray behavior with more accuracy.
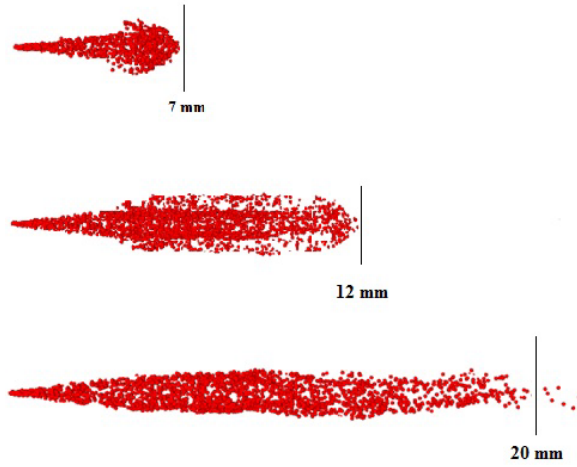
Figure 6. Single hole nozzle, Lagrangian particles depicting penetration layer growth using the Modified Aachen Surrogate at $dx = 0.0625$ mm

Surrogate Grid Convergence (Two-Hole Nozzle)

The effect of multi-hole, in this case two-hole adjacent nozzle, is investigated to numerically seek grid-convergence behavior. A grid converged model will define the resolution required in carrying out well resolved simulations. This configuration features two emerging plumes at different orientations. They are denoted in terms of degrees as plume 0 degree (vertical) and plume 60 degree (adjacent),and both have a manufacturer provided included angle of 159 degrees.

Figure 7a-b presents the effect of spray liquid and vapor behavior with increased resolution and comparison to experiments using Surrogate-C. The resolution levels selected are for $dx = 0.25, 0.125,$ and 0.0625 mm. Figure 7a (top) shows a variations in liquid phase length for the 0 deg and 60 deg plumes with coarse resolution. This is an effect of grid to spray misalignment which improves as the grid is refined. For a cell size of 0.0625 mm both plumes show similar behavior in liquid phase penetration establishing the grid criteria for two-hole plumes. At the finest scales, Figures 7a-b, both show differences with the measurements. The discrepancies in measurements and modeling are for 2 mm and 4 mm in the liquid phase and vapor phase, respectively. Note that this is the current results using the RANS methodology and will be interrogated further with LES; however, RANS is able to capture the overall behavior with a good degree of accuracy.

Figure 8 shows the behavior of the Modified Aachen surrogate from the same grid sensitivity study. Similar results are obtained showing large discrepancies for coarse cell ($dx = 0.25$ mm*)* sizes, improvements for $dx = 0.125$ on the 60 degree plume, and a complete attenuation of the grid effect for the finest cell size
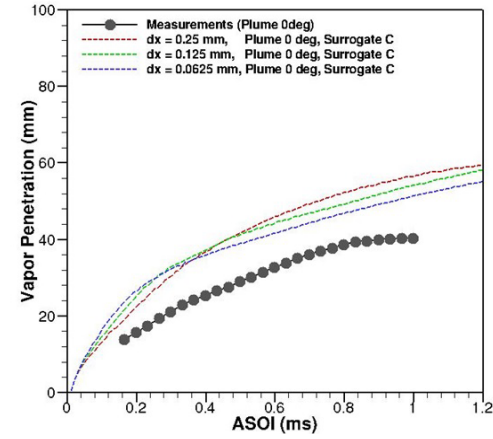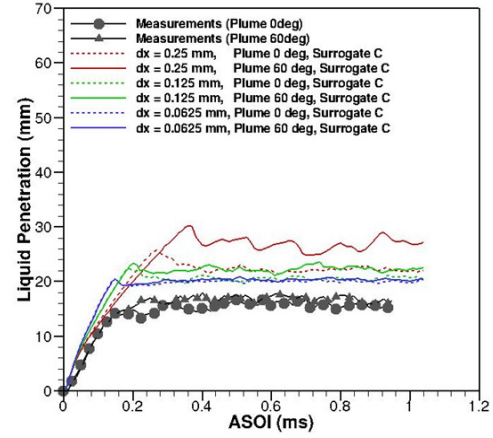

Figure 7. Surrogate-C, two-hole nozzle, grid convergence behavior with liquid (a) and vapor (b) penetration profiles.
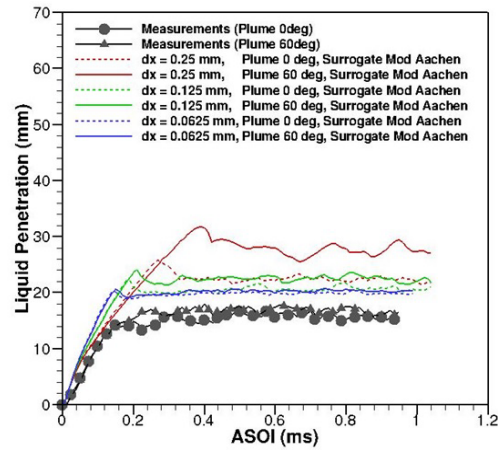

Figure 8. Surrogate-Modifed Aachen, two hole nozzle, grid convergence behavior with liquid penetration profile

($dx = 0.0625$ mm). Vapor phase grid-analysis results show similar behavior as with Surrogate-C.

Figure 9 presents the computed spray structure at times 5, 12, and 40 μs after start of injection. The liquid phase behavior is clearly demonstrated for each

9

nozzle orifice with the correct orientation. The vertical line drawn on each plume marks the computed liquid lengths for each case. Note that this is the result of a RANS turbulence modeling approach with Lagrangian particle spray visualization.
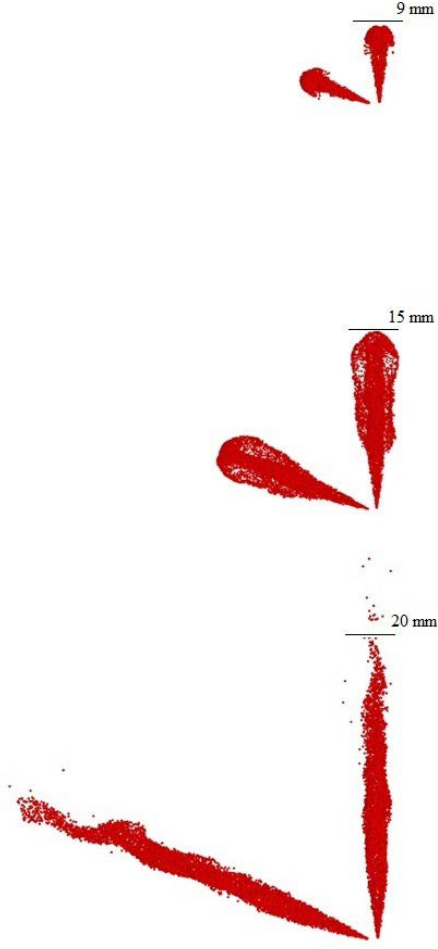

Figure 9. Surrogate-Modified Aachen, two hole adjacent orifice nozzle, Lagrangian particles depicting liquid penetration layer growth in spray formation, $dx = 0.0625$ mm.

Large Eddy Simulations Results

This section present the results obtained using the dynamic structure LES model described in the numerical methodology section. A fine base grid cell size of $dx = 0.0625$ mm with 800,000 total injected parcels for each plume was utilized, AMR criteria for evaporating sprays was based on velocity variations. A total of 9 independent simulations (9 cycles) were carried out for each experiment resulting in averaged profiles for liquid and vapor phase penetrations. This choice was based on the previous work by Senecal et al [7] where it was reported that a total of 9 cycles were needed as the minimum number of LES realizations to

maintain a reasonable representation of the average spray behavior for the Spray A configuration (the average of 9 LES realization will have a mean absolute error of less than +/- 2.0 m/s and 0.005 for velocity and mixture fraction, respectively, 95% of the time). In this section, JP-8 fuel is modeled by selection of the Aachen surrogate. Note also the LES spray breakup time constant used was $B_1 = 5$.

Single-hole LES results are presented in Figure 10a-b showing each LES cycle realization in light red line along with the averaged quantities in solid red line and comparison with experiment.
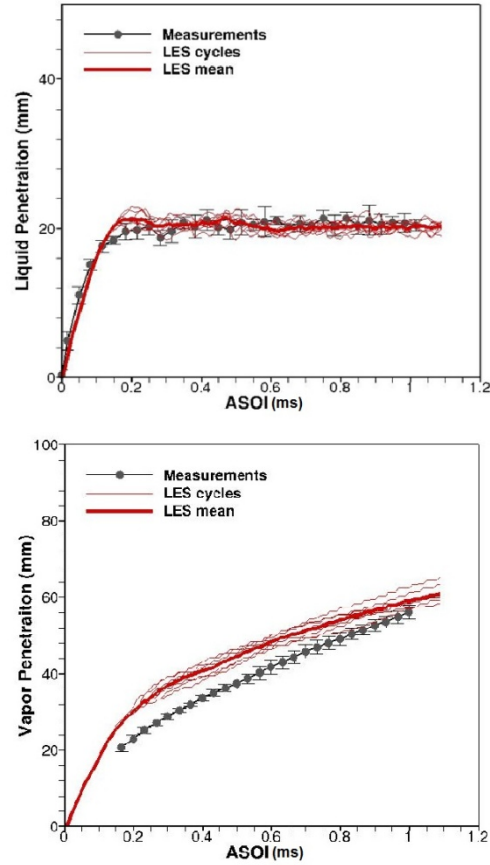

Figure 10. Single hole LES results using the Dynamic Structure model (dx = 0.0625 mm) liquid phase (a) vapor phase (b) penetration

For the single-hole nozzle the results show good agreements for liquid phase length profiles, and moderate success with vapor phase. The vapor phase discrepancies are larger at earlier times and decrease to less than 2% difference at 1 ms (this may be due to the use of single component fuel compared to the real fuel in the experiment (Different evaporation rates). At this point the modeling results are within experimental uncertainty. Additional single-hole results are presented and visually compared to measurements in Figure 11a-b. The experimental data shows the liquid and vapor phase lengths by using a Mie (liquid) and schlieren

(vapor) technique for visualization and are shown side by side with LES results. In this Figure, the modeling results present the velocity contours and shows a peak velocity of 500 m/s at the injector nozzle followed by a typical radial Gaussian velocity distribution and decay in the axial direction. The vapor phase here is depicted as a solid black line surrounding the turbulent plume region, the imaging times are 33, 165, 495, 891, 1188 μs. Figure 12a-d presents the spray's overall mixing and scalar behavior in terms of the mixture fraction, temperature, turbulent kinetic energy, and vorticity at the same time intervals as Figure 11. In Figure 12a, mixture fraction distributions also follow a Gaussian type profile with peak values ($Z = 0.4$) at the centerline near the orifice and decaying radially at fixed times and axially as time progresses. Figure 12b shows the pre-heated fuel entering the chamber with a rail pressure of 1000 bar while undergoing strong mixing with heated ambient at $T_\infty = 900\ K$. To elucidate further on the turbulence transport and mixing process, Figure 12c-d show the turbulent kinetic energy and vorticity contours. The contours show the turbulent kinetic energy mechanism to be dominant in the spray centerline due to the high pressure injection process. The emerging spray interacts with quiescent ambient air which in turn generates the 3D surface instabilities that lead to the spray breakup behaviors. Vorticity dominates in this core region due to the entrainment of air, and mixing, as a result of the injected fuel. This analysis provides a complete picture of the spray breakup and mixing process for single-hole nozzle case.

The two-hole nozzle orifice was also modeled using the LES approach. Equal spatial resolution (dx = 0.0625 mm) and time averaging (9 cycles) techniques were utilized as the single-hole case to provide comparable results. The number of injected parcels was kept fixed as the single-hole value of 800,000 per hole or total 1.6 million in order to accurately resolve the parcel's hydrodynamic effects on the mesh. In particular, we note from experiments that scaling of the injected mass is non-linear leading to a relative decrease in rate of injection (ROI) peak profile magnitude. It is also observed that the ROI profiles used in this study was the average from the two orifices as the present measurement system provides total quantities.

Figure 13a-b shows the instantaneous liquid penetration lengths in red light lines, alongside the mean profile in red solid line, and its comparison to uncertainty quantified measurements. Note that the modeled instantaneous penetration profiles feature larger fluctuations in liquid phase length when compared to the single-hole profiles for both plumes. This could arise from potential insufficient parcel number distributions not scaling with the values from the single-hole case. The averaged value is consistent between both plumes at 20 mm and is an over prediction to experiments by 3-4 mm to the uncertainty region. When compared to single-hole experiments, the mean LES liquid penetration profiles show similar behavior. This implies that there is not much of an impact in liquid length when injecting with single and multi-hole nozzles at this particular orientation (60 degrees, approximately 1 mm apart).
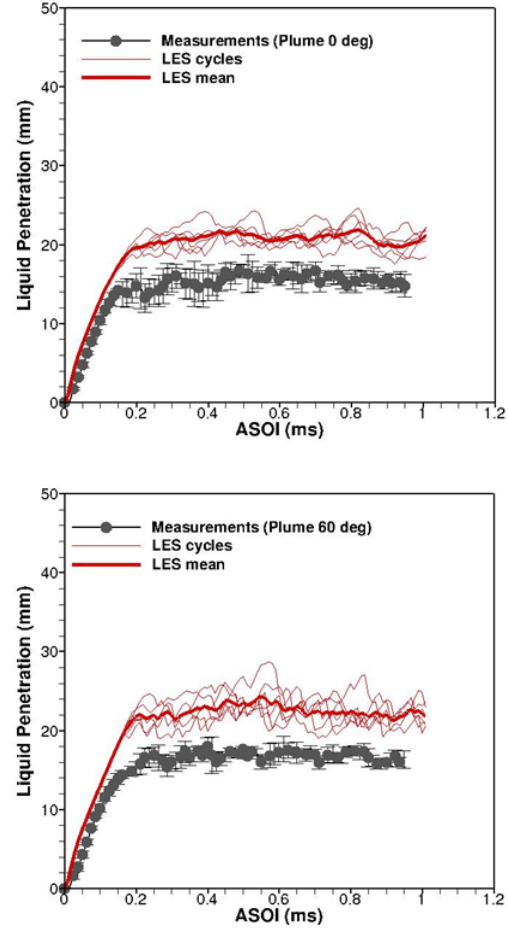

Figure 13. Two hole nozzle, LES liquid penetration profiles using the Dynamic Structure model (dx = 0.0625 mm) for plume 0 deg (a) and plume 60 deg (b).

Figure 14 shows an ensemble of 9 vapor length LES realizations, the resulting LES mean profile, and its comparison to experiments. There are significant differences (~ 8 mm) in the vapor mixing behavior with experiments which results in a similar trend observed in two-hole RANS simulations. In Figure 15 the calculations are compared to experimental Mie Scattering images in an axial orientation at selected times.
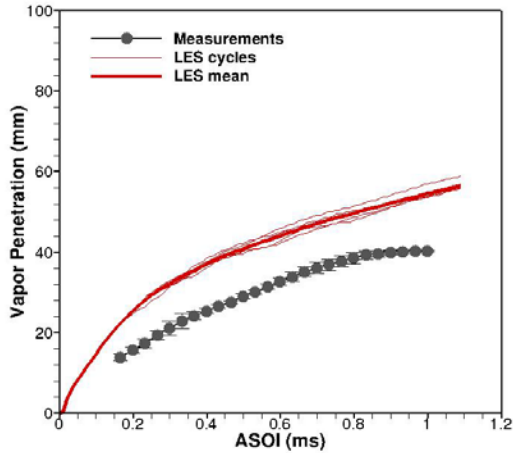
Figure 14. Two hole nozzle, LES vapor penetration profiles using the Dynamic Structure model ($dx =$ 0.0625 mm)

The interpretation of the results between single-hole and multi-hole nozzle configuration requires consideration of several critical injector components. Atomization in sprays is highly dependent on the upstream conditions that occur inside the nozzle structure such as cavitation and turbulence (physical effects) and fluid-structure interaction (interfacial effect). The internal nozzle flow and passage through orifices plays a critical role in determining the rate of injection profiles, injected mass, and other relevant spray quantities. Needle motion in the lateral direction (wobble) has been reported for rail pressures of 1000 bar or greater. This effect has a strong impact on the emerging spray as the needle wobble can potentially and cyclically obstruct fuel passageways. For sprays emerging from two adjacent orifices, there is an additional geometrical asymmetry leading to pressure disturbances that may be preventing the flow to be distributed into the orifice channels uniformly. In Lagrangian modeling of sprays, as is the present effort, the spray is specified from point sources and imposing a Bernoulli type injection velocity derived from ROI profiles, injection quantities, and discharge characteristics. Hence, the internal flow details occurring upstream of the spray injection region are not modeled. It is thought that these effects are prominent for two-hole (asymmetrical) nozzles where the interaction between the needle and displaced fluid and orifice location is vastly different than the single-hole case.

Conclusions

In this study we have conducted validated numerical simulations (low and high fidelity) while demonstrating several numerical and physical effects. The numerical consistency of the solver has been demonstrated by conducting in-depth grid-sensitivity

studies ranging from 0.25 mm to 0.0625 mm, or d_n/dx_i ratios of 0.588 to 2.352. Successful solutions were obtained with resolution levels of 0.125 mm for the single-hole spray while 0.0625 mm were needed for the two-hole spray. The additional level of resolution needed to resolve the multi-hole spray arises from spray's orientation relative to the numerical grid. Because the grids are not perfectly aligned in this case, numerical dissipation effects may emerge causing unphysical behavior with coarse cell sizes.

Two liquid surrogates, Surrogate-C and Modified Aachen Surrogate, were used to model JP-8 fuel. Their selection was based on the literature for gas-phase combustion and also demonstrates their applicability in the liquid phase. Results show consistent behavior among the surrogates. This was demonstrated in the grid sensitivity analysis as both surrogates converged to the same values as the resolution was increased. The behavior of the surrogates also showed good agreements with the spray measurements. Moreover, it was established that, B_1, the temporal spray breakup constant required adjustments when changing from diesel fuels where $B_1 = 7$. The single-hole axial spray configuration was used as the calibration platform for JP-8 fuel resulting in calibration of the spray temporal breakup constant: $B_1 = 10$ (RANS), and $B_1 = 5$ (LES). This is in an agreement to previously developed physical property correlations with B_1 where it was shown to be dependent on mass-density, viscosity, and surface tension. It is also noted that when using high fidelity models the RANS constant must be recalibrated with experiments as it was reported here.

Low fidelity models for both single and multi-hole simulations show good comparisons with experiments in terms of global properties. Because of the coarseness of RANS approach dissipation will dampen out the velocity fluctuations leading to inaccuracies in velocity magnitudes. High fidelity, LES, models are able to capture transients and are a useful tool to provide insights into the underlying dynamics. Using the LES model the interactions between two adjacent plumes, 60° apart, were found to be weak in terms of affecting the penetration profiles. This was concluded after reporting no significant change in liquid penetration for single and two-hole nozzles numerically with a mean value of 20 mm for both cases and similar vapor profiles. The experimentally reported decrease in liquid penetration magnitude from single to two-hole nozzles can be partly due to non-linear behavior in injected mass quantities (and resulting ROI) that was observed in Figure 2. In particular for asymmetrical orifice configurations, such as the two-hole 60 degree nozzle, local Bernoulli type pressure disturbances near the sac volume may arise and result in non-uniform flow distribution. The interaction between the needle, the fluid, and the micro-channels may be particularly

12

complex in this case resulting in the observed injection quantities and spray behavior.

Future work is aimed at explaining some of the reported differences by conducting a deeper investigation with that particular nozzle geometry. Detailed nozzle flow calculations can be carried out to extend the modeling and include the internal flow dynamics, fluid structure interaction between needle and fuel, and the emerging spray. In terms of promoting enhanced plume to plume interactions and mixing, additional work will also address the effect of using cluster nozzles. Optimization studies with respect to the number of cluster used, position, and operating conditions will be carried out to provide cluster arrangements.

In summary, some of the major findings in this study are as follows:

1. Successful grid converged solutions can be obtained for single-hole and multi-hole sprays considering the challenges imposed by the miss-alignment between the spray and the grid (for multi-hole spray). The methodology for grid-converged solution was established previously [7] and has been applied in this paper for multi-hole nozzles.

2. Similar behavior between Surrogate-C and the modified Aachen Surrogate was established both numerically and physically with good agreements with measurements. Note that H/C ratio is maintained fairly uniform across surrogate mixtures in comparison to JP-8 with H/C value of 1.91.

3. Single-hole LES results demonstrates close agreements with measurements with JP-8 sprays. Liquid and vapor penetration length predictions indicate classical high-pressure spray features beginning with a highly transient initial stage and reaching a steady condition for liquid penetration only. Vapor penetration (and mixing) is an inherently dynamic process.

4. Multihole LES results show the effect of two adjacent plumes to be weak at 60 degrees with 1mm hole-to-hole spacing with respect to the liquid penetration profiles. The decrease in experimental liquid penetration length is partly attributed to a decrease in injected mass per hole as compared to the single hole, and to internal flow dynamics and interaction with needle.

References

1. Kweon, C.-B.M., "A Review of Heavy-Fueled Rotary Engine Combustion Technologies," US Army Research Laboratory Technical Report, ARL-TR-5546.

2. Meijer, M., Somers, B., Johnson, J., Naber, J., Lee, S.-Y., Malbec, L.M., Bruneaux, G., Pickett, L.M., Bardi, M., Payri, R., Bazyn, T., *Atomization and Sprays* 22:777–806 (2012).

3. Pickett, L.M., Genzale, C.L., Bruneaux, G., Malbec, L.-M., Hermant, L., Christiansen, C., Schramm, J., *SAE* 2010-01-2106 (2010).

4. Senecal, P., Richards, K., Pomraning, E., Yang, T.,*SAE* 2007-01-0159 (2007).

5. Som, S, Aggarwal, S.K., *Atomization and Sprays* 19(9): 885-903 (2009).

6. Senecal, P, Pomraning, E., Richards, K., Som, S., *Proceedings of the ASME 2012 Internal Combustion Engine Division Fall Technical Conference,* Vancouver, BC, Canada, September 2012.

7. Senecal, P, Pomraning, E, Xue, Q, Som, S., *Proceedings of the ASME 2013 Internal Combustion Engine Division Fall Technical Conference, Dearborn, Michigan, USA, October,* 2013.

8. Xue, E.P, Som, S, Senecal, P., *ILASS Americas, 25th Annual Conference on Liquid Atomization and Spray Systems,* Pittsburgh, PA, May 2013.

9. Habchi, C, Bruneaux, G., *ICLASS, 12th Triennial International Conference on Liquid Atomization and Spray Systems*, Heidelberg, Germany, September, 2012.

10. Kurman, M, Bravo, L, Kweon, C, Tess, M., *Submitted to the 26th Annual Conference on Liquid Atomization and Spray Systems*, Portland, Oregon, May 2014.

11. Pomraning, E, Rutland, C.J., *AIAA Journal,* 40:4 (2012).

12. Pomraning, E., "Development of Large Eddy Simulation Turbulence Models",PhD Thesis, University of Wisconsin-Madison, 2000.

13. Issa, R.I., *Journal of Computational Physics*, 40: 62 (1985).

14. Reitz, R.D, and Diwakar, R., *SAE* 870598, (1987).

15. Bravo, L, Kweon, C., "A Review of Liquid Spray Models for Diesel Engine 3D-CFD Analysis", Submitted to US Army Research Laboratory Technical Report ARL-T14-134-S.

16. Edwards, T, Maurice, L.Q., *Journal of Propulsion and Power,* 17:2 (2001).

17. Colket, M, Edwards, T, Williams, S, Cernanskym N.P., Miller, D.L, Egolfopoulos, F, Lindstedt, P, Seshadri, K, Dryer, F, Law, C, Friend, D, Lenhert, D, Pitsch, H, Sarofim, A, Smooke, M, Tsang, W, *45ᵗʰ AIAA Aerospace and Sciences and Exhibit*, Reno, Nevada, 2007.

18. Edwards, T., Maurice, L.Q., *Journal of Propulsion and Power,* 17:2461-466 (2001).

.
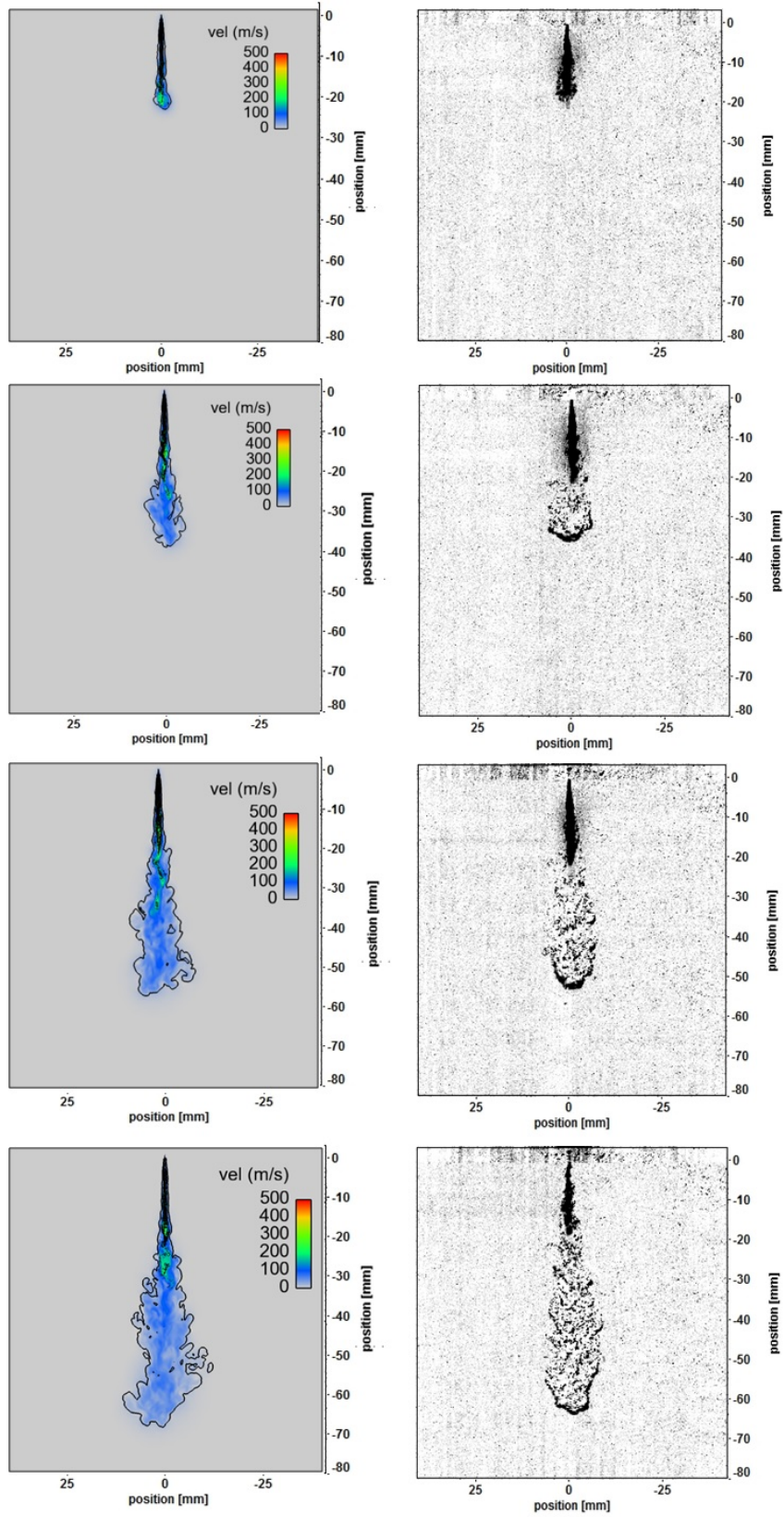
Figure 11. Comparison of Single Hole, dynamic structure LES model (left column) with experiments (right column) at times: 33, 165, 495, 891, 1188 μs.
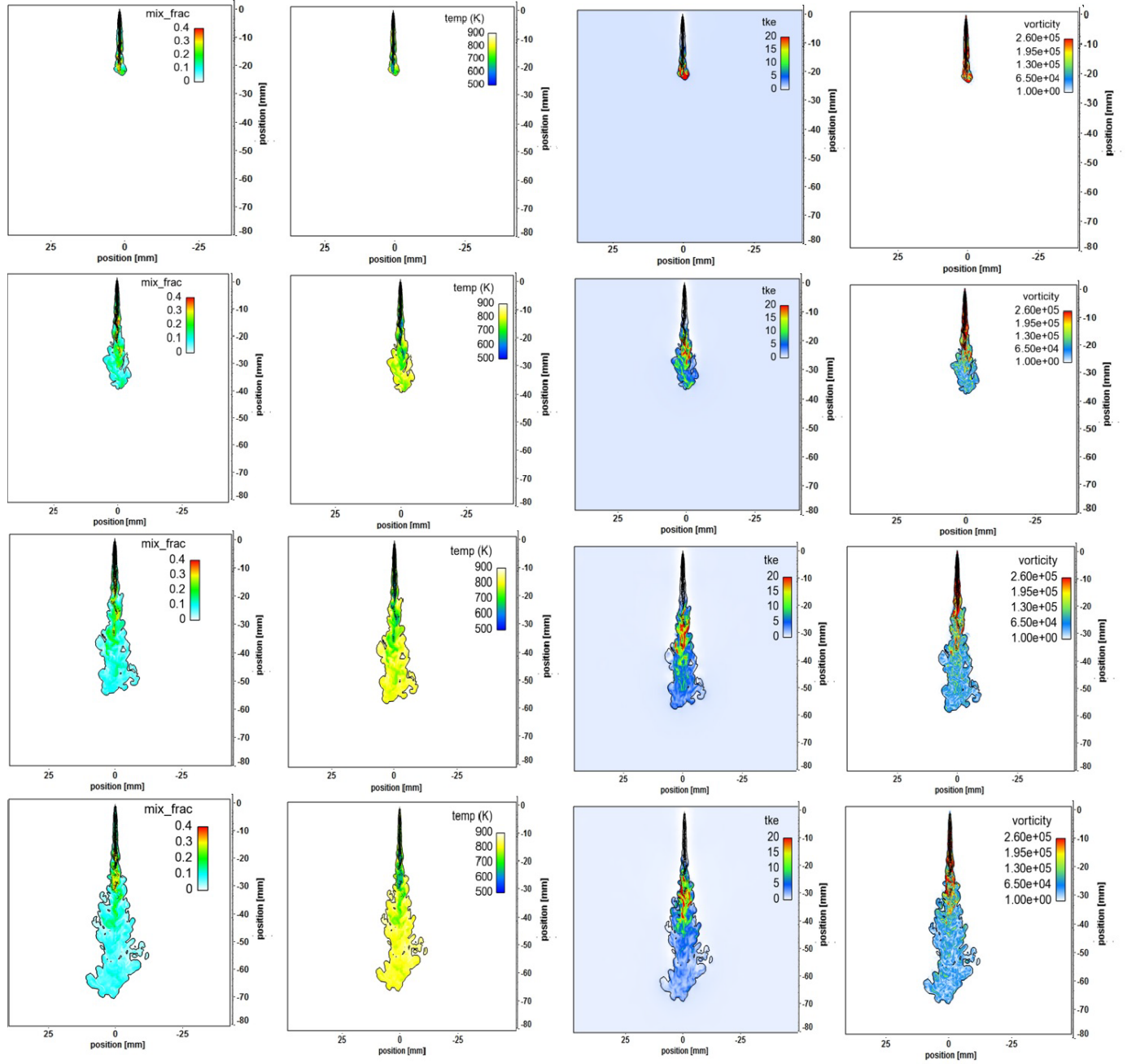
Figure 12 1. Evaporating JP-8 spray, single hole nozzle, configuration modeled via dynamic structure LES at times: 33, 165, 495, 891, 1188 μs. Mixture fraction (1st column), Temperature (2nd column), Turbulent Kinetic Energy (3rd column), Vorticity (4th column)
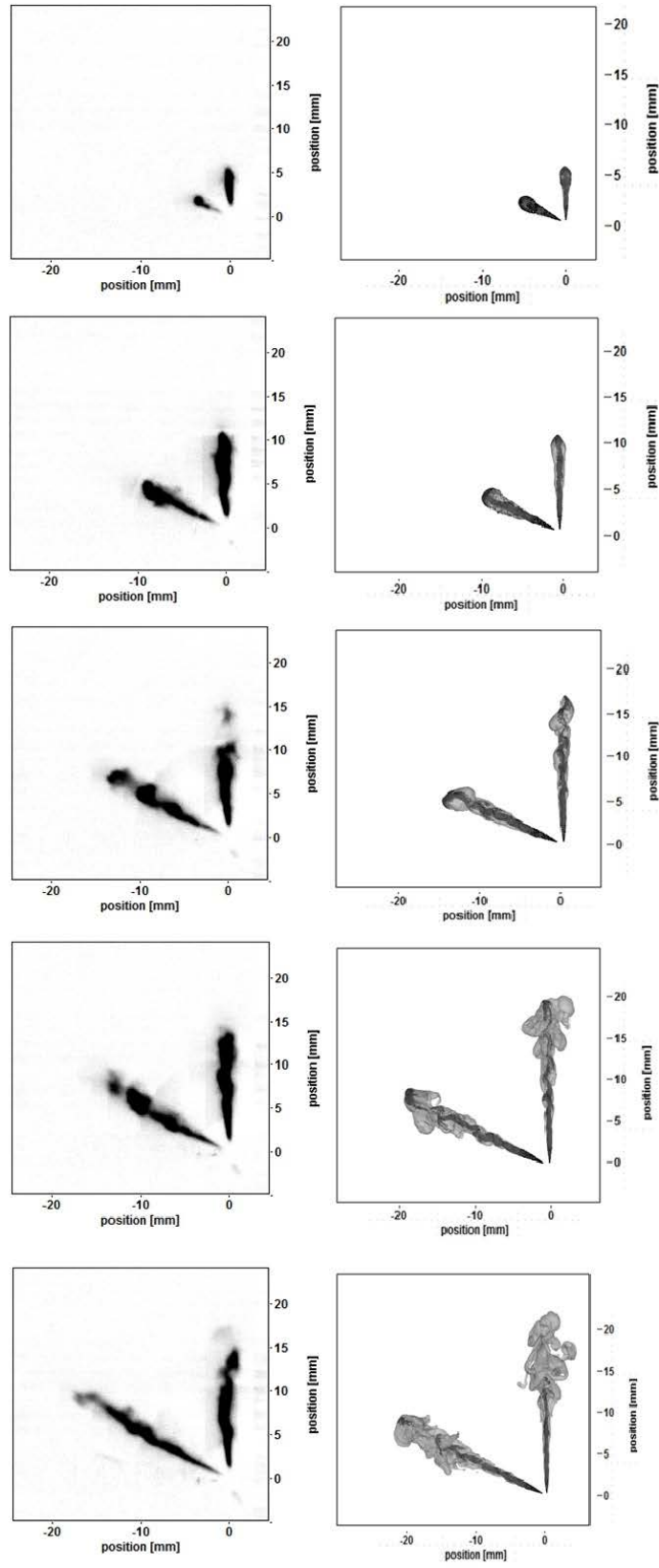
Figure 15. Evaporating JP-8 spray, two hole nozzle, configuration modeled via dynamic structure LES at times: 50, 100, 150, 250, 250 μs. Comparison between experiments liquid length (left column) and instantaneous LES results (right columns) – Liquid length is represented by particles and the 3D vapor iso-surface is shown on grey.